Talanta 209 (2020) 120565

Contents lists available at ScienceDirect

Talanta

journal homepage: www.elsevier.com/locate/talanta

Toward a novel framework for bloodstains dating by Raman spectroscopy: How to avoid sample photodamage and subsampling errors

Alicja Menżyk[a,*], Alessandro Damin[b], Agnieszka Martyna[a], Eugenio Alladio[b,c], Marco Vincenti[b,c], Gianmario Martra[b], Grzegorz Zadora[a,d]

[a] Institute of Chemistry, University of Silesia in Katowice, Szkolna 9, 40-007, Katowice, Poland
[b] Department of Chemistry, University of Torino, Via P. Giuria 7, 10125, Torino, Italy
[c] Centro Regionale Antidoping e di Tossicologia "A. Bertinaria", Regione Gonzole 10/1, 10043, Orbassano, Torino, Italy
[d] Institute of Forensic Research, Westerplatte 9, 31-033, Krakow, Poland

ARTICLE INFO

Keywords:
Bloodstains
Forensic dating
Raman spectroscopy
Rotating stage
Regularized MANOVA

ABSTRACT

Answers to questions about the time of bloodstains formation are often essential to unravel the sequence of events behind criminal acts. Unfortunately, the relevance of preserved evidence to the committed offence usually cannot be verified, because forensic experts are still incapable of providing an accurate estimate of the bloodstains' age. An antidote to this impediment might be substituting the classical dating approach – founded on the application of calibration models – by the comparison problem addressed using likelihood ratio tests. The key aspect of this concept involves comparing the evidential data with results characterizing reference bloodstains, formed during the process of supervised ageing so as to reproduce the evidence. Since this comparison requires data that conveys information inherent to changes accompanying the process of blood decomposition, this study provided a Raman-based procedure, designated for probing into the chemistry of ageing bloodstains. To circumvent limitations experienced with single-point measurements – the risk of laser-induced degradation of hemoglobin and subsampling errors – the rotating mode of spectral acquisition was introduced. In order to verify the performance of this novel sampling method, obtained spectra were confronted with those acquired during conventional static measurements. The visual comparison was followed by analysis of data structure using regularized MANOVA, which boosted the variance between differently-aged samples while minimizing the variance observed for bloodstains deposited at the same time. Studies of relation between these variances demonstrated the superiority of novel procedure, as it provided Raman signatures that enabled a better distinction between differently-aged bloodstains.

1. Introduction

A blood trace deposited at a crime scene, a real treasure trove for forensic experts, is often considered as the main driving force beyond the development of criminal investigations. This is because properly handled blood-related evidentiary material can establish a strong link between an individual and a criminal act or even allow for the reconstruction of bloodshed events, owing to the methods of bloodstain pattern analysis. As a consequence, the wealth of the investigative information, gained by the examination of blood traces, quite often can lead to a major U-turn in a course of forensic proceedings. In certain cases, however, this blood-derived body of data can point the trier of fact in an entirely wrong direction, unless the information about the time of trace formation is provided.

The value of this time-related data and its contribution to criminal investigations are easily comprehensible. Situating blood traces in time can allow to verify the relevance of the preserved evidence to the case at hand or even help in the chronological reconstruction of past events. Unfortunately, confrontation with the issue of time is probably one of the most challenging tasks ever faced by the forensic community [1]. Hence, despite relentless efforts to solve the problem, a reliable method for estimating the time elapsed since bloodstain deposition (or time since deposition, TSD) still remains beyond the reach of forensic science. As it was reported in [2,3], all of already conducted studies have confirmed the time-dependent behaviour of physicochemical properties of blood deposits. Nevertheless, none of developed methods has exhibited the precision and reproducibility regarded as a *conditio sine qua non* of their successful implementation in standard forensic

* Corresponding author.
E-mail address: amenzyk@us.edu.pl (A. Menżyk).

https://doi.org/10.1016/j.talanta.2019.120565
Received 13 June 2019; Received in revised form 7 November 2019; Accepted 12 November 2019
Available online 15 November 2019
0039-9140/

proceedings.

The answer to the question of bloodstains' age, as with all forensic dating tasks, may be considered achievable owing to changes of blood properties that take place during the evidence degradation. Once the bloodstain is created, its initial composition becomes more diverse due to the cascade of physicochemical processes, which involve mainly hemoglobin (Hb) – the dominant component of dried blood traces [2,3]. Redistribution of electrons within π heme's orbitals, as well as changes of the heme pocket geometry that take place during the formation of Hb degradation products (see Fig. S1), trigger conformational rearrangements in polypeptide chains. These subtle structural distortions are reflected in physicochemical properties of bloodstains, which quite easily can be probed with suitable analytical tools [2,3], and subsequently linked to the passage of time.

To date, the vast majority of methods developed for estimating the absolute age of the trace have been guided by one simple principle – they have sought the above-mentioned dependency between the TSD and some dynamic bloodstains properties. In most cases, this task has been completed through the employment of regression analysis, where an equation relating measured values of ageing parameter (i.e. ageing markers) and the absolute age of bloodstains is established [2,3]. However, this approach might be not entirely correct. After all, equations underlying these calibration models, intended for predicting the TSD of questioned materials, always modelled the ageing behaviour of samples that were degrading under tightly-controlled laboratory conditions. And that is what remains the main reason for delayed exploitation of already developed dating methods in routine caseworks. It goes without saying that the crime scene reality hardly ever resembles laboratory settings. The vicissitudes of environment and blood biology mean that no two degradation pathways are exactly alike, and thus using dating models trained on the reference datasets might lead to misestimations of TSD, depriving these conventional methods of almost entire practical value.

It does not mean, however, that, because of these difficulties, questions regarding the time aspect of bloodstains formation should be withdrawn from the courtroom scenario. It just means that these queries should be tackled in a different manner, and exactly this endeavor – the quest for the novel framework for bloodstains dating – constitutes the backbone of the presented research. It is hypothesized that impediments resulting from the variability of ageing kinetics could be addressed by substituting a case-suited comparison problem, considered for example within a likelihood ratio (LR) methodology [4], for the conventional dating approach. The key aspect of this concept is to estimate the (dis)similarity between the stage of evidence degradation and sets of reference materials, obtained through the process of supervised ageing, simulating – as closely as possible – the actual settings of evidence decomposition at the crime scene (Fig. 1). Obviously, in order to enable this comparison, information inherent to changes accompanying the process of blood degradation still have to be delivered,

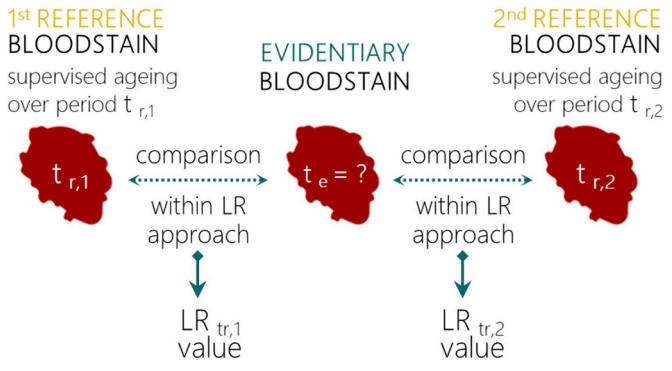

Fig. 1. Likelihood ratio-based approach for estimating the time elapsed since bloodstains deposition (considered as a comparison problem).

therefore the aim of this study was to provide the first component of the aforementioned novel dating approach by developing a Raman-based analytical method, serving as a tool for characterizing the state of bloodstains degradation.

The choice of Raman spectroscopy (RS) is coherent with its maturation as a powerful technique in the analysis of biosamples [5], especially heme-containing proteins [6]. It has been revealed that the vast majority of bands comprising Raman spectra of Hb, isolated erythrocytes and even whole blood originate from vibrational modes involving the C–C, C=C, and C–N bonds of the porphyrin ring within the heme structure [6–8], which are highly sensitive to even minute structural changes of the protein. Thus, this particular feature of hemoproteins vibrational spectra holds promise for adapting RS to bloodstains dating studies, as it should give an insight into formation of different Hb derivatives over time. And indeed, the time-dependent behaviour of Raman spectra of blood deposits has been already demonstrated [9–11]. However, despite this valuable discovery, there are still some challenges that continually hamper implementation of Raman-based methodology in standard proceedings. One of these obstacles might be representative probing of the chemical composition of degrading bloodstains, which is usually pursued through acquisition of a few single-point measurements within different areas of the sample [9–11]. The problem is that dried deposits of body fluids are not only physically, but also chemically heterogeneous, hence this sampling mode might result in poor reproducibility of measurements and, in the long term, misestimations of TSD.

In view of the above, this study intended to expand the current Raman-based approaches largely through eradication of the risk of the laser-induced degradation of bloodstains [3,9,12] and subsampling errors. In order to do so, the rotating measurement mode that involved spinning the bloodstain sample during the spectral acquisition by means of a magnetic-driven sample-holder [13,14] was established, and subsequently employed for characterizing the behaviour of bloodstains during three-week degradation period. To verify the capability of the novel sampling method to provide data that facilitated discerning differently-aged blood traces, its performance was compared with the routinely applied single-point sampling procedure (the static mode).

2. Material and methods

2.1. Sample preparation

All experiments were conducted on blood drawn from a single donor in order to mitigate the possible influence of inter-individual factors on the variability of spectral responses. 20 μL aliquots of capillary blood, obtained by finger puncture, were transferred (without the addition of any preservatives or anticoagulants) into aluminium sample pans – yielding almost featureless background that did not interfere with Raman scattering – and then allowed to dry for two hours before spectrum collection.

During the entire study, two classes of bloodstains were employed. The first class, which was used for conducting experiments for selecting the setup of spectral acquisition, comprised four groups of six bloodstains. Each of these groups served for testing different levels of laser power (for details see *2.2. Raman instrumentation and sample presentation*). Regarding the second class, namely the population of samples used for ageing studies, two separate sets consisting of six bloodstains each, respectively for rotating and static measurement modes, were created. Deposited bloodstains were then stored, protected from any light sources, for three weeks under controlled laboratory conditions (temperature: 23.6 ± 2.0 °C, relative humidity: 30 ± 4%).

All the blood samples were deposited at time intervals so as to compensate the different duration of spectral acquisition in the static and rotating modes, and through that equalize the ongoing transformations of bloodstains, which are particularly rapid at the initial stage of ageing [2,3].

2.2. Raman instrumentation and sample presentation

The spectra were recorded in the range 300–1800 cm^{-1} using a Renishaw inVia Raman Microscope spectrometer, equipped with a 5× objective (with the NA value of 0.1) and a 785-nm laser line. Due to the exceptional susceptibility of Hb to laser irradiation [3,9,12], the rotating measurement mode – aimed at reducing the excitation-induced damages – was introduced and confronted with the conventional single-point measurements. In order to indicate parameters allowing for non-invasive spectral acquisition, the ratio between the band at 1227 cm^{-1} and one of the previously identified Hb aggregation markers [3,12] – a spectral feature at 1248 cm^{-1} – was monitored for four groups of bloodstains, created independently for the static and rotating measurements. Each of these groups were analyzed with increasing power of the excitation source to verify whether upon increasing the power any of the monitored ratios significantly decreased, which would be indicative of laser-induced detrimental effects. The laser beam was focused to a diameter ~72 μm^2 and its power equalled to 0.6 mW ($7.98 \cdot 10^{-3}$ mW/μm^2), 1.2 mW (0.02 mW/μm^2), 5.8 mW (0.08 mW/μm^2) and 11.5 mW (0.16 mW/μm^2) measured at the specimen, which corresponded to 0.5%, 1%, 5% and 10% of the initial power of excitation source (~103 mW on the sample), respectively. Throughout this power test, the exposure time and number of accumulations were adapted separately for each excitation power, so as to maintain the comparable number of counts, and thereby provide Raman spectra of similar signal-to-noise ratio.

2.3. Monitoring the progress of bloodstains degradation

Subsequently, in order to investigate the time-dependent behaviour of bloodstains, samples were analyzed every two hours (from two up to eight hours elapsed since bloodstain formation) and then once per day for the period of three weeks. All of Raman spectra were registered in both measurement modes.

2.4. Data pre-processing

Right at the beginning, the original spectra were truncated to omit the range 300–600 cm^{-1}, which was severely affected by the noise and increasing baseline. As a result, each spectrum covered the range 600–1800 cm^{-1}, which included most of Raman bands associated with the vibrational modes of target analytes (Hb and its derivatives).

Subsequently, in order to mitigate the effect of fluorescence, an adaptive iteratively reweighted penalized least squares (airPLS) fitting procedure, introduced by Zhang et al. [15] was applied. In this technique no user intervention (e.g. band detection) is required, and the baseline itself is gradually approximated by weighted penalized least squares method. Weighting is provided to the sum of squared differences between the original spectrum and the estimated baseline to eliminate the bands and focus only on baseline points during the approximation procedure. Since the performance of this correction method might be negatively affected by noise factors, a third-order Savitzky-Golay filter was applied prior to background subtraction – using 21-point and 17-point windows in case of the static and rotating modes, respectively – and was followed by the logarithmic transformation and mean-centering, aimed at ensuring the homogeneity of data variance.

Finally, in order to alleviate unwanted inter-spectra distortions, and through that reveal genuine temporal behaviour of Raman features, the background-corrected Raman spectra were subjected to the probabilistic quotient normalization (PQN) [16]. During this procedure, the normalization factor for each spectrum was indicated as a median of quotients, which were obtained by dividing the acquired spectrum by a reference (the median signal).

It should be also clearly stated that the choice of the pre-processing strategy was based on the thorough visual inspection of corrected signals. However, the problem of optimizing the spectral pre-processing can be automated, for example by using genetic algorithms [17], which is the subject of our further work.

2.5. Comparison between the performance of the static and rotating sampling modes using rMANOVA

The prerequisite for any effective discrimination is that the average variance of the replicate measurements within each group is much lower than the variance of groups averages. If this condition is not satisfied, distributions of variables characterizing the compared groups will overlap, preventing from successful discrimination. That also applies to LR models [4] designed for distinguishing between differently-aged bloodstains.

Among methods of variance analysis offered by the contemporary chemometrics, there are several tools suited for studying highly correlated multivariate data sets. One of them is a regularized multivariate analysis of variance (rMANOVA), which – unlike its prototype (MANOVA) – is suitable for data populations containing more variables than samples [18]. The main goal of this method is defining new directions (eigenvectors) that boost the between-group variance (denoted as **B**), whilst minimizing the within-group variance (denoted as **W**).

In this study, a single group comprised Raman spectra of bloodstains characterized by the same TSD values, hence the variation within measurements of equally-aged bloodstains corresponded to within-group variance **W**; whilst the between-group variance **B** equalled to the variation of the averages of bloodstains deposited at different time. In order to evaluate the capability of both measurement modes to provide data that facilitate discrimination of bloodstains in terms of their TSD, and, through that to verify which of those two methods (static or rotating) should be implemented in future LR-based dating procedure, rMANOVA was employed to compare the variance structure of registered Raman spectra. Taking into account that in the case of univariate data all matrices are substituted by scalars (e.g. **B** becomes b^2), the b^2 to w^2 ratio was investigated on the first eigenvector (first canonical variate, CV1), being the direction maximizing the b^2/w^2.

Additionally, static and rotating datasets comprising spectra registered over whole degradation period (three weeks) were divided into three subgroups, corresponding to spectra acquired within the first seven, 14 and 21 days of degradation. For each of these subgroups the b^2/w^2 were calculated, so as to investigate the changes of the performance of both modes with progression of time.

All the mathematical background of the research was carried out using the R software (version 3.3.1) [19].

3. Results and discussion

3.1. Optimization of a Raman spectra acquisition setup

The motivation for choosing the 785-nm excitation was threefold. First of all, owing to the previous studies of Lemler et al. [9] and the group of Sato [20], it has been demonstrated that the Raman spectrum of whole blood acquired with 785 nm laser line, does not provide information about any other of its constituents but our target analytes – Hb protein and its derivatives. Secondly, exploiting the laser wavelength distant from the electronic absorption region of fluorescent components of blood allowed to avoid overlapping the photoluminescence phenomenon with the informative Raman scattering. And finally, it was also crucial to ensure that the process of spectral acquisition did not alter the Hb, which is known for its susceptibility to photodegradation [9,12,21]. The exploitation of excitation source outside the range of electronic transitions of Hb derivatives, which include weak Q-band (α and β) between 490 and 650 nm, and the most intense Soret band in the region of 400–436 nm [2,3], allowed to reduce the risk of the increased absorption of the electromagnetic radiation, with consequent heating of the sample, triggering formation of

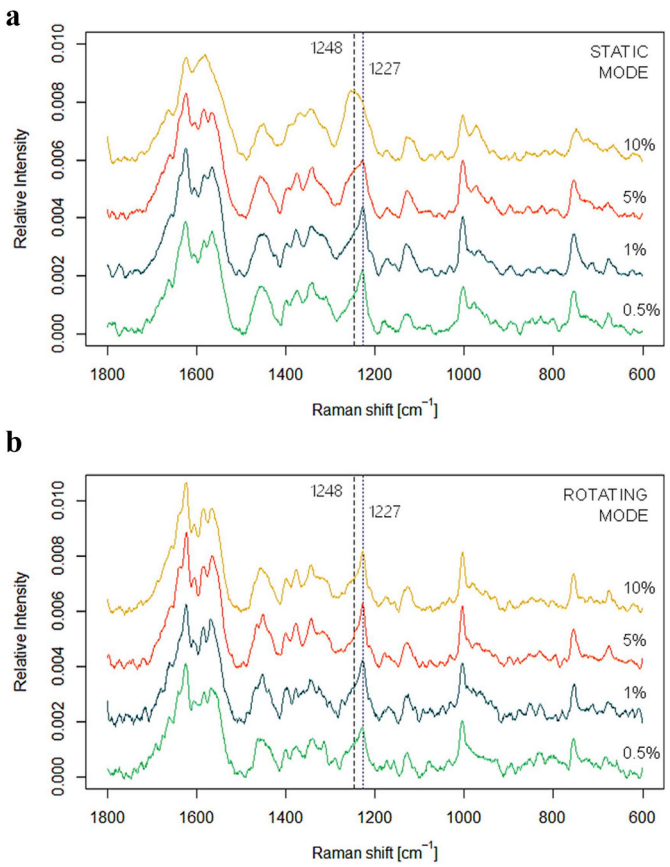

Fig. 2. Influence of the laser power on Raman spectra of 2-h bloodstains registered with 785 nm excitation laser in the (**a**) static and (**b**) rotating mode. The ratio between intensities of heme aggregation marker at 1248 cm^{-1} (dashed line) and a stable band at 1227 cm^{-1} (dotted line) served as an indicator of Hb photodegradation while deciding on non-invasive measurement parameters. Spectra were treated according to the procedure set forth in *2.4. Data pre-processing* and shifted for better visualization.

undesirable laser-induced heme aggregation products [12,21].

Nonetheless, the above-mentioned precaution against forced degradation of bloodstains might not be sufficient, because the photoinduced denaturation can appear within the nominally non-resonant region of Hb, even if using laser irradiation of relatively low power [9,12]. An example of such an undesired effect is depicted in Fig. 2a, which illustrates spectral symptoms attributed to the laser-triggered degradation that occurred while performing measurements of the static sample with 785 nm excitation. The sudden change of spectral features can be clearly observed for spectra of static bloodstains registered with 0.16 mW/μm^2 and 0.08 mW/μm^2 (respectively 10% and 5% of initial laser power), however to a much lower level. The Raman signature of photodegraded bloodstain consists of increased background counts (not indicated in Fig. 2a) and broader spectral features in comparison to those registered with lower levels of laser power, namely $7.98{\cdot}10^{-3}$ mW/μm^2 and 0.02 mW/μm^2 (0.5% and 1%). In addition, changes in the relative intensity of several spectral components occurred – in particular the increase of bands at 1248 cm^{-1} and 974 cm^{-1}. Taking into account the structure of Hb, a few hypotheses regarding the possible mechanism behind laser-induced degradation can be proposed, fortunately a closer inspection of spectra provides some possible answers. As Raman signatures of laser-damaged bloodstains were deprived of the band at 1357 cm^{-1} – which is an oxidation state marker indicative of the Fe^{2+} ion embedded within heme structure – it could have been ruled out that the degradation mechanism led to dissociation of oxygen from oxyHb as described in [22], giving rise to deoxyHb (Fig. S1). That conclusion is coherent with work of Black et al. [23,24], who investigated chemical changes in blood undergoing laser photocoagulation. In case of these studies, authors did not observe any liberation of free oxygen from the blood samples, and hence assumed that the oxygen became irreversibly, chemically bound in the Fe^{3+} metHb complexes. Ramser et al. [21] came to the similar conclusions, suggesting the formation of metHb as the final step of the photoinduced changes. Firstly, however, calculations of heat transfer in red blood cells (RBCs) were performed in order to verify whether the observed spectral changes could have resulted from thermal processes initiated by light absorption. Eventually, thermal degradation was excluded as an explanation of the observed spectral alterations, as an estimated rise of the temperature at the laser focus equalled ~2.3 °C (for initial laser power 0.7 mW), hence – according to these estimations – the actual cell temperature remained well below physiological conditions (~37 °C). These calculations, however, had taken into account the water as a main absorbing component of blood, disregarding the contribution of Hb – highly concentrated in dried bloodstains – which absorption coefficient at the NIR region is much higher than that of water. Given that information, the hypothesis about the potential mechanism behind the laser-triggered degradation should be reverified once again, possibly by resorting to the previous findings of Monash group [25,26]. This time, the increased intensities of bands at 972 cm^{-1}, 1248 cm^{-1} and 1366 cm^{-1} were attributed to the formation of Hb aggregates resulting from photoinduced Hb denaturation, whilst the enhanced background was interpreted as a consequence of the proximity of aggregated heme structures, which facilitated migration of energy, in the form of an exciton, throughout that closely packed protoporphyrin moieties [25,26]. These spectral characteristics were also consistent symptoms of laser-induced degradation observed in case of our study – primarily the enhanced intensities of 974 cm^{-1} and 1248 cm^{-1} bands as well as increased background counts – hence it is reasonable to postulate the possible involvement of protein denaturation in laser-triggered degradation of bloodstains. It should be also emphasized that registered Raman signals do not allow to unambiguously identify which of the degradation products dominate the composition of photodamaged bloodstains. Consequently, the exact mechanism behind laser-induced degradation is only hypothesized and needs to be examined further. In order to get more complete picture, it would be advisable to facilitate the reasoning process with other analytical techniques, which are well-recognized tools, capable of characterizing the Hb derivatives (e.g. UV–Vis spectroscopy). Nevertheless, among all of those questions, there are few certainties, and one of them is that care must be taken to prevent the photoinduced chemistry of Hb.

In this study, the decision on non-invasive parameters of spectral acquisition was adopted based on information encoded in the signal at 1248 cm^{-1}, serving as a marker of laser-induced degradation. Apart from the evident power-dependent behaviour of 1248 cm^{-1} band, the choice of this particular degradation indicator was also justified by the chemistry underlying its occurrence. In recent studies of Lednev's group [10,11] this spectral feature was assigned to the frequency of amide III band – interpreted as being indicative of random coil conformation of Hb protein – which led authors to the conclusion that the process of Hb denaturation preceded aggregation. And indeed the region of amide III vibration, which serves as a sensitive probe of peptide conformation, has been defined within 1260–1310 cm^{-1}, 1235–1242 cm^{-1} and 1240–1250 cm^{-1} for α-helix, β-sheet and random coil structure, respectively [27–29], thus it might be an appealing idea to interpret the band that appears at ~1248 cm^{-1} as the amide III mode. This reasoning, however, most likely is incorrect, since the protein spectral features are not always observed in the Raman signatures of erythrocytes or whole blood. That is because the obtained spectrum is the superimposition of all vibrationally active constituents, and in some cases a tremendous enhancement of certain Raman intensities may be observed – depending on the applied excitation source – due to the resonance Raman effect. It should be borne in mind that because of the resonant enhancement of hemoporphyrin modes, the bands originating

from proteins do not appear in the spectra recorded at 488, 514, 568 and 633 nm, contrary to the signals registered with 1064 nm lasers that give insight into the secondary structure of proteins [30]. And in fact, the assignment of the ~1248 cm^{-1} band proposed by Doty et al. [10,11] was based on the spectral characteristics of proteins acquired with 1064 nm [29], and not 785-nm laser, which was actually employed by authors during the dating studies of bloodstains [10,11]. Comparing to the NIR (1064 nm) laser source, the situation is somewhat different in case of 785-nm excitation, where a few proteinaceous bands appear, such as the amide I (1650 cm^{-1}), the CH_2/CH_3 deformation modes originating from amino acid side chains at 1446 cm^{-1}, and the phenylalanine band at 1003 cm^{-1}. However, the whole spectral range between 1200 and 1300 cm^{-1} – and thus also the 1248 cm^{-1} degradation marker – which in fact overlays with the region of amide III modes, have been also assigned to the C_m–H methine vibrations within protoporphyrin IX moiety of heme [9,26,31–34], which are of B_{1g} and E_u symmetry type. These bands, as evidenced by the study of Wood et al. [26], are strongly enhanced – along with A_{1g}, A_{2g}, B_{2g} and vinyl modes (see Table S1) – once the Raman signal is acquired using 785-nm laser excitation. Since the enhancement mechanism within heme groups has a greater impact on the Raman spectrum than the contribution of protein bands such as amide III, hence in our case (and also in case of Lednev's group studies [10,11]) the spectral feature observed at ~1248 cm^{-1} is associated with the C_m –H in plane vibrations of methine hydrogen in porphyrin macrocycle.

Considering the above, it is perfectly reasonable to apply the 1248 cm^{-1} band as a sensitive molecular probe of Hb perturbations in response to the laser power, as the C_m–H methine vibrations within the protoporphyrin structure might be affected by heme stacking and protein interactions that take place during the process of its degradation. Having looked at spectra in Fig. 2a it becomes clear that if one aims at obtaining good-quality Raman signatures while avoiding the photodamage of Hb, high power coupled with short acquisitions should be substituted by low excitation power combined with long acquisition times. Precisely for this reason, application of conventional static mode, when monitoring the time-dependent behaviour of heterogeneous materials, might pose some technical difficulties. And that is because providing a representative Raman signature, which in case of single-point measurements can be only obtained by performing multiple measurements across the sample, is hardly possible within short space of time. Fortunately, the problem of laser power and interconnected time resolution can be mitigated by a relatively simple solution applied in this study – implementation of rotating measurement mode [13,14]. Since in this case the irradiated point of the bloodstain is being constantly refreshed, the excitation energy is distributed over a larger area, hence the risk of sample damaging can be significantly reduced. And indeed, the visual examination of Raman spectra registered for rotating samples (Fig. 2b) revealed that even the signals acquired with 10% of initial laser power (0.16 $mW/\mu m^2$) were deprived of spectral features typical of decomposed bloodstains. The difference in the trends, qualitatively determined by direct inspection of sets of data as those in the panels of Fig. 2, were fully confirmed by calculating the ratio between the band at 1227 cm^{-1} and the aforementioned modification marker at 1248 cm^{-1} for all sets of measurements. The results of these calculations are presented in the form of ratios distribution (boxplots) in Fig. 3. Therefore eventually, the signal acquisition in the static mode was performed using ten 20-s accumulations with 1% (0.02 $mW/\mu m^2$) and in the rotating mode – two 20-s accumulations with 10% of initial excitation laser power (0.16 $mW/\mu m^2$) – since both of these setups allowed to reduce to a minimum duration of spectral acquisition, whilst mitigating the detrimental influence of the laser.

3.2. Visual inspection of time-dependency of bloodstains Raman spectra

Having established the procedures of static and rotating sampling methods, the study entered the next phase, which was solely devoted to monitoring the ageing behaviour of blood traces. The most prominent time-dependent trend, readily observed among registered signals, was an increase of baseline intensity (Figs. S3a and S3c). Unfortunately, the root cause of this phenomena as yet has not been fully explained, and there are at least a few possible explanations for the observed substantial background.

As already established, oxyhemoglobin (oxyHb) – or more precisely heme embedded within its structure – could not have been the origin of observed fluorescence. Admittedly, porphyrins and among them a precursor of heme – protoporphyrin IX – exhibit fluorescence when excited in the NIR range, however this emission is significantly quenched when the tetrapyrrole ring is bound to iron ions [3]. Consequently, fresh whole blood does not exhibit NIR autofluorescence [35], in contrast to degraded bloodstains [9–11,36–38]. As evidenced also in case of this research, the fluorescence enhancement of blood deposits was constantly progressing over time, which suggested that one of the possible origin of this phenomenon was accumulation of degradation products exhibiting higher intrinsic fluorescence than oxyHb. Owing to the previous studies [35,39,40], it was established that one of those Hb derivatives – showing strong fluorescence emission [12] – are hemichromes (Fig. S1), which were identified among products of natural [9] as well as laser-induced [12] degradation of blood. At the moment, it also cannot be entirely excluded that hemichromes are not the only dysfunctional forms of Hb generated during the ageing process. Perhaps the decomposition continue progressing, giving rise to other acutely degraded Hb derivatives. As previously noted, decomposed Hb exhibits fluorescent properties, resulting possibly from the dissociation of Hb subunits followed by the release of iron ions [35,39,40]. In order to complete the picture, it should be also added that electron spin resonance studies of bloodstains had previously revealed signal, allegedly originating from non-heme iron, which was increasing with degradation time [41]. In light of the above, it is hard to escape the impression that this degradation pathway would somehow resemble the *in vivo* blood recycling process, where Hb protein is metabolized to globin chains and heme [35,39–41]. Due to this heme breakdown, iron is released, hence Hb metabolites show significant fluorescence. As yet, however, it has been neither confirmed, nor denied if this type of decomposition can proceed *ex vivo*, because the issue of whether heme degradation is solely enzymatic or also non-enzymatic remains unresolved [41,42]. On the other hand, the observed background interference does not really have to be connected solely to the intrinsic fluorescence of degradation products. Another possible explanation should be sought in numerous studies of Wood et al. [25,26,31,32], who established that the same effect of a marked increase in background counts can be also present due to excitonic interactions that take place throughout the network of heme aggregates. Admittedly, these observations were made during rather invasive measurements, which among other things intended to investigate the effect of laser power and temperature on Raman signals of RBCs. However, it was already demonstrated that the Raman spectra of laser-damaged bloodstains bore more than a passing resemblance to naturally-aged specimens [9], suggesting that both degradation mechanisms give rise to similar decomposition products. If that is the case then the process of bloodstains ageing should lead to aggregation of similar dysfunctional forms of Hb, increasing the probability of excitonic interactions between the metalloporphyrins, which manifest themselves in a gradual increase of baseline. An alternative hypothesis – somewhat similar to the above explanation, as once again linked to the process of Hb aggregation – was presented in the studies of Marzec et al. [43]. It was reasoned that such substantial background may originate from the photothermal signal [44], as photons absorbed by Hb proteins are converted into heat, which eventually might be blamed for the enhanced spectral baseline. In other words, the older the bloodstain, the more advanced the process of Hb aggregation and, through that, the increase of baseline intensity. Taken together, there is no doubt that further studies to understand the origin of background influence are

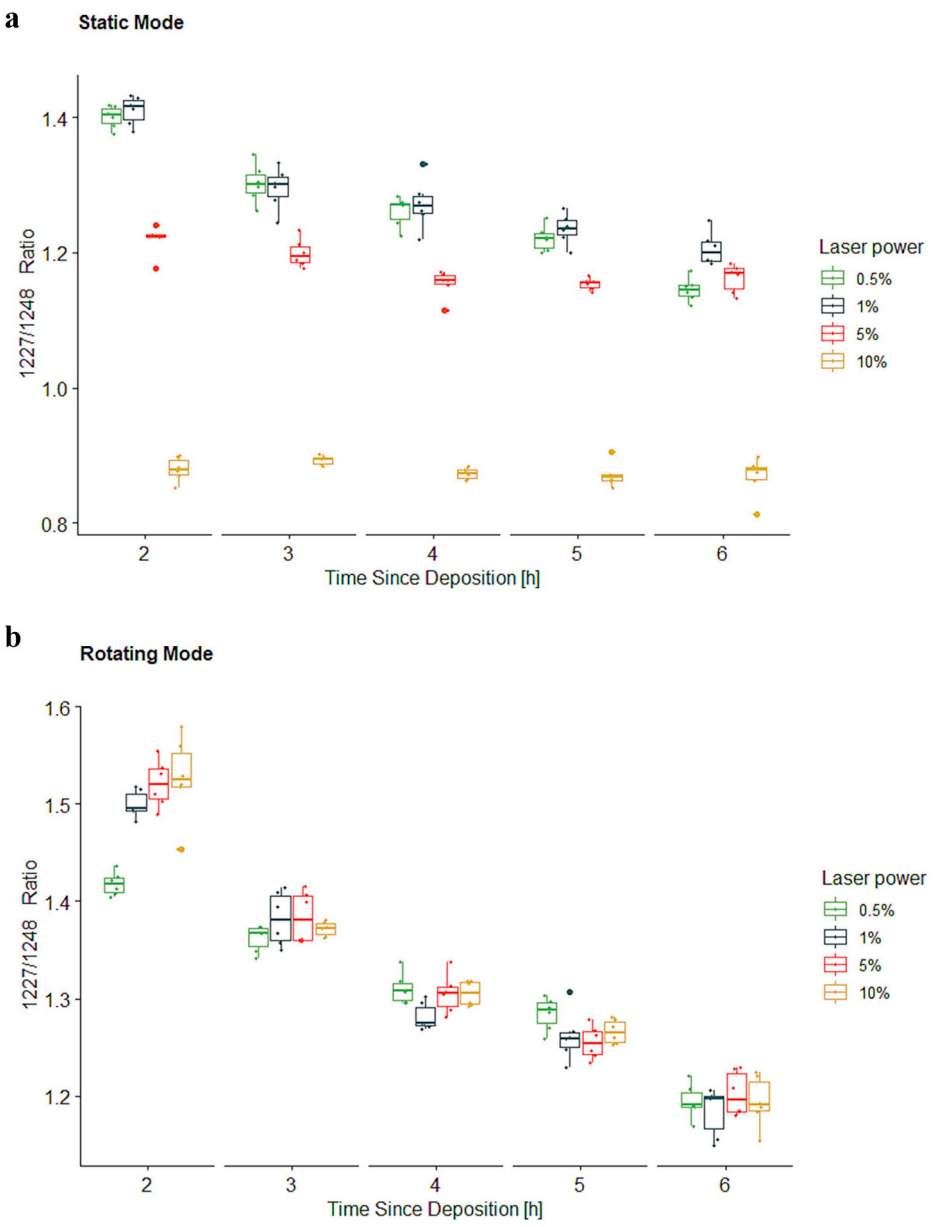

Fig. 3. Boxplots depicting the distribution of intensity ratios between peaks located at 1227 cm^{-1} and 1248 cm^{-1}, serving as markers of Hb photo-damage, observed for Raman spectra of bloodstains registered using different levels of laser power – $7.98{\cdot}10^{-3}$ $mW/\mu m^2$, 0.02 $mW/\mu m^2$, 0.08 $mW/\mu m^2$ and 0.16 $mW/\mu m^2$ corresponding to 0.5%, 1%, 5%, 10% of initial power – in the (**a**) static and (**b**) rotating measurement mode.

required. At the moment, however, it seems reasonable to postulate that the observed phenomenon might be in fact an interplay between the intrinsic fluorescence of degradation products (e.g. hemichromes) and aggregation of Hb species inside bloodstains, resulting in excitonic interactions and more profound photothermal effect due to increased absorption of photons.

Nevertheless, inferring about bloodstains TSD solely from the fluorescence signal, increasingly dominating the Raman scatter, is rather risky, simply because variation in the baseline may also derive from factors other than formation of degradation products (e.g. changing sampling geometry). Therefore, prior to further data analysis, spectra were baseline corrected to expose changes within Raman bands, which co-evolved with the fluorescence enhancement. The effects of this correction procedure are presented in Fig. S3.

A pictorial view of the background-corrected Raman signals (Fig. 4) revealed subtle, but noticeable alterations appearing in bands pattern as a function of time. Once again our attention was drawn mainly to changes occurring in the range of 1220–1300 cm^{-1}, which bore a strong resemblance to laser-induced spectral distortions (compare with Fig. 2a). A distinctive and relatively sharp band at about 1227 cm^{-1} was broadening with progression of time, moving through maximum reached at ca. 1248 cm^{-1} to end up forming a band at 1255 cm^{-1}. As already broadly discussed in *3.1. Optimization of a Raman spectra acquisition setup*, the origin of this temporal behaviour should be attributed to alterations of C_m–H methine vibrations within heme moiety [25,26]. By plotting the time behaviour of ratios of bands at 1227 cm^{-1} and 1255 cm^{-1} (Fig. 5), called later 1227/1255 ratio, it can be clearly observed that rapid decrease of their value within first few days of degradation would allow to distinguish between differently-aged bloodstains. This differentiation would be more effective in case of rotating mode, as no overlap between distributions of ratios corresponding to different time-points was observed contrary to static bloodstains (see, for instance, pairs of data at 4 and 6 h, and at 6 and 8 h) which was the initial evidence of superior reproducibility of spectra obtained using the novel sampling mode.

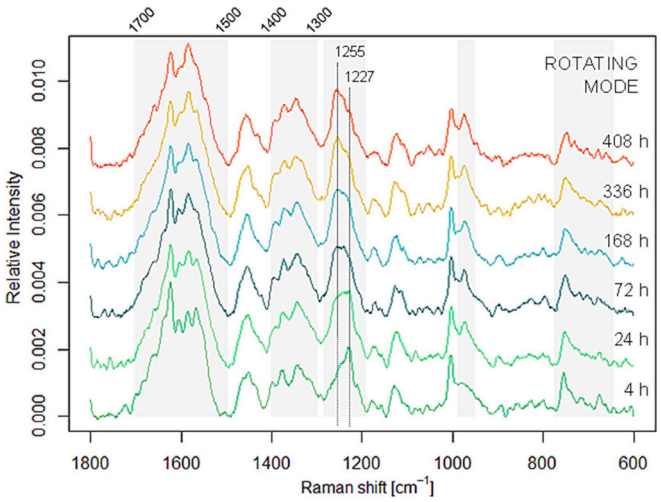

Fig. 4. Exemplary Raman signatures of ageing bloodstains registered with 785 nm excitation laser in the rotating mode (an equivalent of this plot corresponding to the static mode can be found in Fig. S4). Time-dependent bands are indicated in grey. Spectra were treated according to the procedure set forth in *2.4. Data pre-processing* and shifted for better visualization.

3.3. Variance analysis with rMANOVA – comparison between the static and rotating mode

Notwithstanding the evident time-dependent behaviour of the monitored 1227/1255 ratio, its adoption in dating task has some obvious limitations. First of all, the manual rating of the bloodstains' age through this particular spectral feature is not applicable at long time scales, as the ratio values level off rather quickly – in case of this study after c.a. 168 h (seven days) of natural degradation (Fig. 5). Besides, inferring the TSD from the changes of 1227/1255 ratio limits dating capabilities of the method, as it considers information encoded in a single spectral feature, while ignoring the interactive effects of other potentially informative dynamic variables.

In order to indicate any other time-changes in registered Raman spectra, and through that verify whether further distinction between similarly-aged bloodstains would be achievable, the inspection of b^2/w^2 values corresponding to each value of Raman shift was performed (Fig. 6). A listing of these time-dependent spectral features, characterized by values of b^2/w^2 above unity, was gathered in Table S1. As it can be seen, b^2/w^2 values close to zero are present in positions typical of bands attributable to non-heme related Hb constituents – such as amide I (1655 cm^{-1}) or CH_2/CH_3 amino acid deformation modes (1450 cm^{-1}), indicating that this structural motifs of Hb remained rather stable in time. For the rest, apart from the broadly discussed 1220–1300 cm^{-1} region, the variation between spectra of differently-

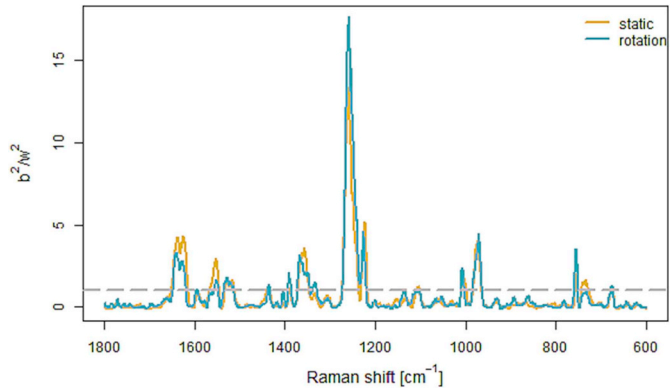

Fig. 6. The b^2/w^2 values corresponding to each value of Raman shift. Grey dashed line indicates $b^2 = w^2$.

aged bloodstains appeared to be primarily due to changes observed at higher Raman shifts – ranges of 1700–1500 cm^{-1} and 1400–1300 cm^{-1} – which are known to contain so-called core-size and oxidation markers of Hb [8], respectively. The first group of mentioned Raman bands gives an insight into porphyrin distortions that accompany changes of the central porphyrin-core size and the spin state of iron ion, the second is sensitized to alterations in the electron density in the π heme's orbitals [8]. For instance, the intensities of such spectral features as 576 cm^{-1} [ν(Fe–O_2)] and 420 cm^{-1} [δ(Fe–O–O)] – both of them non-indicated in the spectra – as well as a characteristic band of Fe^{2+}–O_2 at 1638 cm^{-1} [$\nu(C_\alpha C_m)_{asym}$] decreased over time. According to these observations, the Hb forms, in which an oxygen binds to the sixth vertical coordination position of the iron ion of heme (oxyHb) were disappearing during decomposition process (Fig. S1). By contrast, already mentioned heme aggregation markers (974 cm^{-1}, 1255 cm^{-1}) were increasing over degradation time, and at the initial stage of ageing they were present on the spectra along with the Fe^{2+}–O_2 marker band at 1638 cm^{-1}, indicating that the bloodstains contained a mixture of aggregated heme and oxyHb. Furthermore, the range of so-called oxidation markers (1400–1300 cm^{-1}) was consistently dominated by the band at 1376 cm^{-1} – the marker of oxidation state corresponding to Fe^{3+} – suggesting that the population of ferric-heme species (e.g. metHb and hemichromes) was towering over the ferrous Hb derivatives (Fig. S1). All these factors combined are strong indicators that the ageing of blood traces boils down primarily – though not necessarily exclusively – to the conversion of oxyHb to metHb and HC, followed by the aggregation of heme species. It should be also noted that the spectra of whole blood samples at advanced stage of natural degradation exhibit the same vibrational features as are observed for the dried fresh whole blood, exposed to high laser powers (λ_{ex}: 785 nm). This is in agreement with previous results of Lemler et al. [9], who reported that

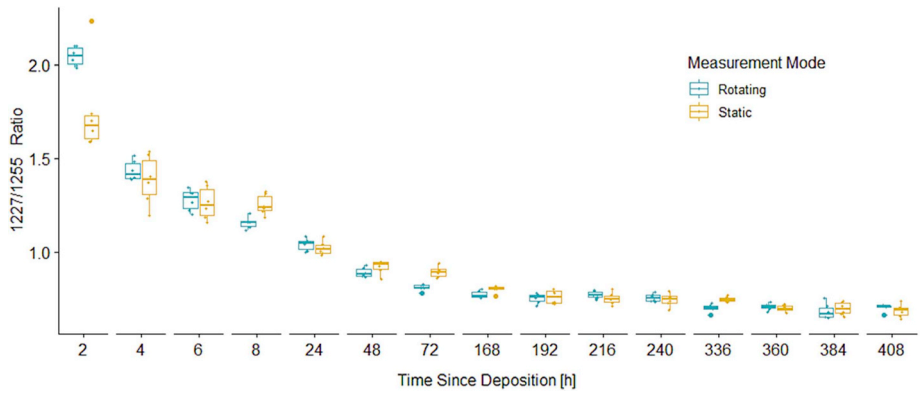

Fig. 5. Boxplots representing intensity ratios of Raman bands at 1227 cm^{-1} and 1255 cm^{-1} against the age of static and rotating bloodstains (given in hours).

the natural as well as the laser-induced deterioration of blood give rise to similarly structured degradation products. Obviously, exhaustive characterization of the ongoing degradation mechanisms and resulting decomposition products based solely on the near-infrared Raman spectra is rather difficult. Part of the reason is that the ageing process of blood led to the increased background counts, which might have obscured observation of some small changes in incredibly complex signals that may be crucial for understanding the role of other possible pathways of the *ex vivo* degradation of bloodstains. A potential solution might be application of more advanced methods of mathematical modelling, such as multivariate curve resolution-alternative least squares (MCR-ALS) proposed by [45], which performs deconvolution of Raman spectra in order to enable identification of significant spectral components responsible for ageing process. Nevertheless, at this point of our study, it is important to comprehend that detailed exploration of ageing mechanisms was never the main motivation behind this research. The fundamental idea was to establish a non-invasive tool, capable of providing an insight into the degree of bloodstains degradation in a relatively quick and highly-representative manner. The crucial piece of information here is that Raman spectra exhibit clear time-dependency, and these changes in spectral characteristics are well-recognized effects of the formation of Hb degradation products [9–12], which can be mathematically correlated with the elapsed time and subsequently employed in forensic dating studies.

Having demonstrated that Raman spectra of ageing bloodstains provide a wealth of chemical information, hidden within hundreds spectral features other than 1227/1255 ratio, the discrimination capabilities of both measurement modes were examined in depth using rMANOVA, which took into account correlation among these variables. In agreement with data in Fig. 5, the calculated b^2/w^2 along CV1 demonstrated that the rotating mode of spectral acquisition was indisputably better than the conventional procedure in terms of its potential discriminating capabilities, because higher values of ratios were obtained (see Fig. 7). Indeed, the movement of the sample allowed to provide, at given time-point, truly averaged spectral characteristics of chemically heterogeneous bloodstain, which was reflected in low rates of w^2, characterizing dispersion of measurements of the blood samples with the same TSD.

Furthermore, the differences between the groups of bloodstains varying in TSD were most pronounced on the scale of the first week, when the ongoing degradation changes were escalating. For both modes, during the very first few days of ageing, the highest b^2/w^2 values were observed. However, owing to more effective reduction of within-group variability in case of the novel sampling mode, ratios corresponding to rotating measurements were almost twice as high as those characterizing the static dataset. Therefore, especially in the initial stage of the ageing, when the conventional single-point measurements are particularly vulnerable to subsampling errors, employment of rotating mode should be the most beneficial. As time progressed and degradation ceased, the gradual decline in b^2/w^2 values was noted. In addition, differences between ratios obtained for static and rotating modes were diminishing, because the distributions of degradation products along the surface of bloodstains were getting more and more uniform. Nevertheless, despite the decrease of degradation rate, it was demonstrated that discerning differently-aged bloodstains would be still possible ($b^2 > w^2$), and, what is even more important, the superiority of rotating mode in terms of this discriminating capability was clearly demonstrated within the entire degradation period (Fig. 7). This, in turn, heralds successful implementation of newly developed Raman-based procedure in the LR-based comparison approach for estimating time elapsed since bloodstains deposition.

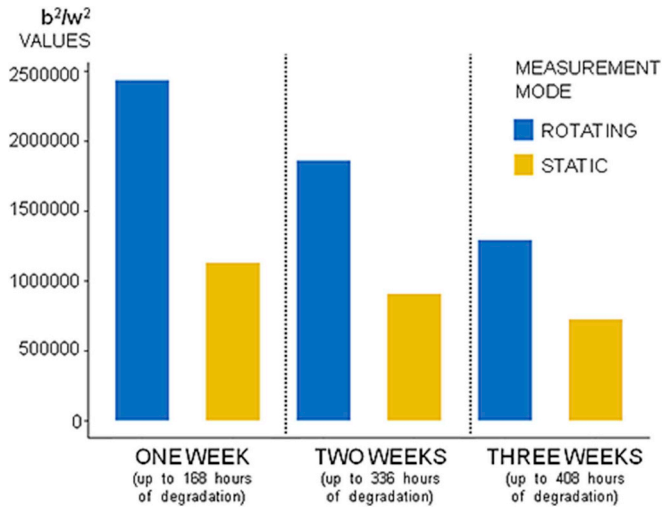

Fig. 7. Comparison of b^2/w^2 values (on the first eigenvector, CV1) characterizing data sets obtained in rotating and static mode after one, two and three weeks of bloodstains degradation.

4. Conclusions

The comparison of signals registered in the rotating mode with those acquired for static bloodstains demonstrated that the former sampling method should be preferred over the conventional measurements for two reasons. First of all, as regards the reproducibility of obtained spectral signatures, the rotating mode allowed to reduce the risk of subsampling errors. This point was objectively confirmed by the analysis of data using rMANOVA, which revealed that, in case of rotating mode, the variance between Raman spectra registered for bloodstains deposited at the same time (w^2) was significantly lower than the variance observed between spectral signatures of differently-aged blood traces (b^2). It means that the novel sampling method contributed to exposing the genuine time-related changes in the Raman spectra whilst reducing the variability resulting from the inhomogenity of the probed sample, and thereby facilitated the discrimination of bloodstains varying in TSD. This level of representativeness simply could not have been achieved through the performance of repeated static measurements in different areas of the sample. Especially, if the analysis should be carried out in the shortest possible time, as is the case with monitoring the initial stage of ageing process. Which brings us to the second reason behind advocating for the rotating mode, namely the duration of measurements. Since the application of the spinning device allowed to constantly renew the irradiated area of bloodstains, the laser-induced damaging of the specimen could have been decreased to a negligible extent. This, in turn, made it possible to register the Raman spectra using higher laser power, leading to the reduction in the length of measurements, down to 6 min in comparison to the conventional static approach, lasting 15 min.

However, even though the conducted study allowed to place the rotating mode of Raman spectroscopy among front-line analytical tools capable of providing chemical insight into the time-dependent behaviour of bloodstains, it cannot be denied that there is more to evidence dating than simply collecting data. And even though establishing an analytical method itself is far from being straightforward, practical implementation of proposed methodology in criminal proceedings is wholly more challenging.

As with all forensic tasks, an elastic dating approach that takes into account all the factors influencing the validity of the evidence evaluation is the key to success. Unfortunately, no two crime scenes are ever exactly the same, and neither is the ageing kinetics of blood traces. Precisely for this reason, establishing a universal framework for TSD estimations may be cumbersome, if not impossible to accomplish. So, despite technological advances, the question remains – how to incorporate the uncertainty deriving from the influence of factors affecting the ageing processes into the dating approach? It appears virtually impossible, but also somehow unreasonable to develop in

advance dating models for each possible scenario that could be encountered at a hypothetical crime scene, hence the solution should be sought elsewhere, perhaps by looking at the dating problem from an entirely different perspective. Our future studies will be therefore primarily focused on reframing the issue of evidence dating by substituting the LR-based comparison procedure for conventional calibration models, which eventually may re-shape our notion of what is achievable in terms of the evidence dating.

Notes

The authors declare no competing financial interest.

Acknowledgements

We would like to acknowledge the Reviewer for valuable comments and suggestions, which helped to improve and clarify the manuscript.

This research did not receive any specific grant from funding agencies in the public, commercial, or not-for-profit sectors.

Appendix A. Supplementary data

Supplementary data to this article can be found online at https://doi.org/10.1016/j.talanta.2019.120565.

References

[1] C. Weyermann, O. Ribaux, Situating forensic traces in time, Sci. Justice 52 (2012) 68–75.
[2] R.H. Bremmer, K.G. de Bruin, M.J.C. van Gemert, T.G. van Leeuwen, M.C.G. Aalders, Forensic quest for age determination of bloodstains, Forensic Sci. Int. 216 (2012) 1–11.
[3] G. Zadora, A. Menżyk, In the pursuit of the holy grail of forensic science – spectroscopic studies on the estimation of time since deposition of bloodstains, TrAC Trends Anal. Chem. (Reference Ed.) 105 (2018) 137–165.
[4] G. Zadora, A. Martyna, D. Ramos, C. Aitken, Statistical Analysis in Forensic Science: Evidential Value of Multivariate Physicochemical Data, Wiley, Chichester, 2014.
[5] H.J. Butler, L. Ashton, B. Bird, G. Cinque, K. Curtis, J. Dorney, K. Esmonde-White, N.J. Fullwood, B. Gardner, P.L. Martin-Hirsch, M.J. Walsh, M.R. McAinsh, N. Stone, F.L. Martin, Using raman spectroscopy to characterize biological materials, Nat. Protoc. 11 (2016) 664–687.
[6] C.G. Atkins, K. Buckley, M.W. Blades, R.F.B. Turner, Raman spectroscopy of blood and blood components, Appl. Spectrosc. 71 (2017) 767–793.
[7] S.Z. Hu, K.M. Smith, T.G. Spiro, Assignment of protoheme resonance Raman spectrum by heme labeling in myoglobin, J. Am. Chem. Soc. 118 (1996) 12638–12646.
[8] D.L. Rousseau, M.R. Ondrias, Raman scattering, in: D.L. Rousseau (Ed.), Optical Techniques in Biological Research, Academic press, inc., Orlando, 1984, pp. 100–108.
[9] P. Lemler, W.R. Premasiri, A. DelMonaco, L.D. Ziegler, NIR raman spectra of whole human blood: effects of laser-induced and in vitro hemoglobin denaturation, Anal. Bioanal. Chem. 406 (2014) 193–200.
[10] K.C. Doty, G. McLaughlin, I.K. Lednev, A Raman “spectroscopic clock” for bloodstain age determination: the first week after deposition, Anal. Bioanal. Chem. 408 (2016) 3993–4001.
[11] K.C. Doty, C.K. Muro, I.K. Lednev, Predicting the time of the crime: bloodstain aging estimation for up to two years, Forensic Chem. 5 (2017) 1–47.
[12] R. Dasgupta, S. Ahlawat, R.S. Verma, A. Uppal, P.K. Gupta, Hemoglobin degradation in human erythrocytes with long-duration near-infrared laser exposure in Raman optical tweezers, J. Biomed. Opt. 15 (2010) 055009.
[13] M. Signorile, F. Bonino, A. Damin, S. Bordiga, A novel Raman setup based on magnetic-driven rotation of sample, Top. Catal. 61 (2018) 1491–1498.
[14] A. Damin, et al., European patent No. WO2017077513 (A1), (2017).
[15] Z.-M. Zhang, S. Chen, Y.-Z. Liang, Baseline correction using adaptive iteratively reweighted penalized least squares, Analyst 135 (2010) 1138–1146.
[16] F. Dieterle, A. Ross, G. Schlotterbeck, H. Senn, Probabilistic Quotient Normalization as robust method to account for dilution of complex biological mixtures. Application in 1H NMR metabonomics, Anal. Chem. 78 (2006) 4281–4290.
[17] D.E. Goldberg, Genetic algorithms in search, Optimization and Machine Learning, Addison-Wesley, Berkeley, 1989.
[18] J. Engel, L. Blanchet, B. Bloemen, L. Heuvel, U. Engelke, R. Wevers, L. Buydens, Regularized MANOVA (rMANOVA) in untargeted metabolomics, Anal. Chim. Acta 89 (2015) 1–12.
[19] R. Core Team, R: A Language and Environment for Statistical Computing, R Foundation for Statistical Computing, Vienna, Austria, (2012) 3-900051-07-0http://www.R-project.org/.
[20] H. Sato, H. Chiba, H. Tashiro, Y.J. Ozaki, Excitation wave-length-dependent changes in Raman spectra of whole blood and hemoglobin: comparison of the spectra with 514.5, 720, and 1064 nm excitation, Biomed. Opt. 6 (2001) 366–370.
[21] K. Ramser, E.J. Bjerneld, C. Fant, M. Käll, Importance of substrate and photo-induced effects in Raman spectroscopy of single functional erythrocytes, J. Biomed. Opt. 8 (2003) 173–178.
[22] K.M. Marzec, A. Rygula, B.R. Wood, S. Chlopicki, M. Baranska, High-resolution Raman imaging reveals spatial location of heme oxidation sites in single red blood cells of dried smears, J. Raman Spectrosc. 46 (2014) 76–83.
[23] J. Kehlet Barton, D.P. Popok, J.F. Black, Thermal analysis of blood undergoing laser photocoagulation, IEEE J. Sel. Top. Quant. 7 (2001) 936–943.
[24] J.F. Black, J. Kehlet Barton, Chemical and structural changes in blood undergoing laser photocoagulation, Photochem. Photobiol. 80 (2004) 89–97.
[25] B.R. Wood, L. Hammer, L. Davis, D. McNaughton, Raman microspectroscopy and imaging provides insights into heme aggregation and denaturation within human erythrocytes, J. Biomed. Opt. 10 (2005) 14005–14013.
[26] B.R. Wood, P. Caspers, G.J. Puppels, S. Pandiancherri, D. McNaughton, Resonance Raman spectroscopy of red blood cells using near-infrared laser excitation, Anal. Bioanal. Chem. 387 (2007) 1691–1703.
[27] J.L. Lippert, D. Tyminski, P.J. Desmeules, Determination of the secondary structure of proteins by laser Raman spectroscopy, J. Am. Chem. Soc. 98 (1976) 7075–7080.
[28] H. Ishizaki, P. Balaram, R. Nagaraj, Y.V. Venkatachalapathi, A.T. Tu, Determination of beta-turn conformation by laser Raman spectroscopy, Biophys. J. 36 (1981) 509–517.
[29] A. Rygula, K. Majzner, K.M. Marzec, A. Kaczor, M. Pilarczyk, M. Baranska, Raman spectroscopy of proteins: a review, J. Raman Spectrosc. 44 (2013) 1061–1076.
[30] Y. Ozaki, A. Mizuno, H. Sato, K. Kawauchi, S. Muraishi, Biomedical application of near-infrared fourier transform Raman spectroscopy. Part I: the 1064-nm excited Raman spectra of blood and methemoglobin, Appl. Spectrosc. 46 (1992) 533–536.
[31] B.R. Wood, L. Hammer, D. McNaughton, Resonance Raman spectroscopy provides evidence of heme ordering within the functional erythrocyte, Vib. Spectrosc. 38 (2005) 71–78.
[32] B.R. Wood, L. Hammer, L. Davis, D. McNaughton, Raman microspectroscopy and imaging provides insights into heme aggregation and denaturation within human erythrocytes, J. Biomed. Opt. 10 (2005) 14005–14013.
[33] M. Asghari-Khiavi, A. Mechler, K.R. Bambery, D. McNaughton, B.R. Wood, A resonance Raman spectroscopic investigation into the effects of fixation and dehydration on heme environment of hemoglobin, J. Raman Spectrosc. 40 (2009) 1668–1674.
[34] W.R. Premasiri, J.C. Lee, L.D. Ziegler, Surface-enhanced Raman scattering of whole human blood, blood plasma, and red blood cells: cellular processes and bioanalytical sensing, J. Phys. Chem. B 116 (2012) 9376–9386.
[35] N.M. Htun, Y.C. Chen, B. Lim, T. Schiller, G.J. Maghzal, A.L. Huang, K.D. Elgass, J. Rivera, H.G. Schneider, B.R. Wood, R. Stocker, K. Peter, Near-infrared autofluorescence induced by intraplaque hemorrhage and heme degradation as marker for high-risk atherosclerotic plaques, Nat. Commun. 8 (2017) 1–16.
[36] K. Guo, S. Achilefu, M.Y. Berezin, Dating bloodstains with fluorescence lifetime measurements, Chemistry 18 (2012) 1303–1305.
[37] K. Guo, N. Zhegalova, S. Achilefu, M.Y. Berezin, Bloodstain age analysis: to- ward solid state fluorescent lifetime measurements, Proc. SPIE 8572 (2013) 857214.
[38] S. Mc Shine, K. Suhling, A. Beavil, B. Daniel, N. Frascione, The applicability of fluorescence lifetime to determine the time since the deposition of biological stains, Anal. Methods. 9 (2017) 2007–2013.
[39] U. Neugebauer, A. März, T. Henkel, M. Schmitt, J. Popp, Spectroscopic detection and quantification of heme and heme degradation products, Anal. Bioanal. Chem. 404 (2012) 2819–2829.
[40] E. Nagababu, J.M. Rifkind, Heme degradation during autoxidation of oxyhemoglobin, Biochem. Biophys. Res. Commun. 273 (2000) 839–845.
[41] T. Miki, A. Kai, M. Ikeya, Electron spin resonance of bloodstains and its application to the estimation of time after bleeding, Forensic Sci. Int. 35 (1987) 149–158.
[42] W.H. Schaefer, T.M. Harris, F.P. Guengerich, Characterization of the enzymatic and nonenzymatic peroxidative degradation of iron porphyrins and cytochrome P-450 heme, Biochem. 24 (1985) 3254–3263.
[43] K.M. Marzec, K. Kochan, A. Fedorowicz, A. Jasztal, K. Chruszcz-Lipska, J. Cz. Dobrowolski, S. Chlopicki, M. Baranska, Raman microimaging of murine lungs: insight into the vitamin A content, Analyst 140 (2015) 2172–2177.
[44] D. Zhang, M.N. Slipchenko, D.E. Leaird, A.M. Weiner, J.-X. Cheng, Opt. Express 21 (2013) 13864–13874.
[45] A. Takamura, D. Watanabe, R. Shimada, T. Ozawa, Comprehensive modeling of bloodstain aging by multivariate Raman spectral resolution with kinetics, Comms. Chem. (2019), https://doi.org/10.1038/s42004-019-0217-1.